Formation and accumulation of gas hydrate in porous media

A. W. Rempel[1] and B. A. Buffett

Department of Earth and Ocean Sciences, University of British Columbia, Vancouver, Canada

Abstract. Vast quantities of clathrate hydrate are found in the Arctic and in marine sediments along continental margins. The clathrate structure traps enormous volumes of methane gas, which is both a possible source of global climate change and a potential energy resource. The growth rate and spatial distribution of gas hydrate in the shallow sediments are influenced by a variety of interacting physical processes. In order to quantify these processes, we develop mathematical models for hydrate formation in porous media. An analytical model is derived for the idealized problem of hydrate growth in a porous half-space which is cooled on its boundary. Our calculations predict the growth rate of a hydrate layer for a given rate of cooling and show that the volume of hydrate is strongly dependent on the two-phase equilibrium between hydrate and seawater. For a representative phase diagram we find that the volume of hydrate in the layer is less than 1% of the pore volume. Larger volumes of hydrate observed in some locations demand a sustained supply of gas and a long accumulation time. Numerical calculations are used to investigate situations that are more representative of conditions in marine sediments. A simple theoretical expression is derived for the rate of hydrate accumulation due to advection of methane gas from depth. Using typical estimates of fluid velocities in accretionary environments, we obtain an accumulation rate of 1% of the pore volume in 10^5 years. The predicted vertical distribution of hydrate is consistent with geophysical inferences from observed hydrate occurrences along the Cascadia margin. Similar distributions can arise from the combined effects of in situ methane production and warming due to ongoing sedimentation. Predicted differences between these two formation models may be detectable in geophysical and geochemical measurements.

Introduction

Gas hydrates are ice-like crystalline compounds of water and gas molecules that are stable above 0°C at sufficiently high pressures. They are characterized by a high capacity to store gas; 1 m³ of the typical hydrate found in nature contains as much as 164 m³ of methane gas at standard temperature and pressure conditions [*Kvenvolden*, 1993]. Vast hydrate reserves have been identified in the Arctic [*Collett*, 1993] and beneath the sea floor off continental margins [*Collins and Watkins*, 1985; *Ginsburg et al.*, 1989; *Hyndman and Spence*, 1992; *Kvenvolden*, 1993; *Holbrook et al.*, 1996]. These discoveries have prompted preliminary investigations into the feasibility of extracting methane gas for use as a clean-burning fuel [*Cherskii and Bondarev*, 1972; *Sloan*, 1990;

Collett, 1992] and the effect of a possible release of the gas on global climate [*Nisbet*, 1990; *Paull et al.*, 1991; *Loehle*, 1993]. To quantitatively assess the economic and environmental significance of these gas reserves, we must first understand how the formation conditions influence the rate and distribution of hydrate accumulation.

Most of the ocean floor is within the appropriate pressure-temperature regime for natural gas hydrates to be stable, but adequate gas supplies for hydrate formation are normally confined to continental shelf regions. Within shelf sediments the base of the hydrate stability field is determined mainly by the geothermal gradient; at some depth the temperature must exceed the equilibrium temperature at the in situ pressure. This depth is commonly associated with a discontinuity in acoustic impedance between partially hydrate saturated sediment with a relatively high elastic velocity and fluid-saturated sediment, with a small amount of free gas [*Singh and Minshull*, 1994]. Studies of the resulting seismic reflections, known as bottom simulating reflectors, provide estimates of the hydrate saturation immediately above the base of several hydrate deposits [*Rowe*

and Gettrust, 1993; *Singh and Minshull*, 1994]. Unfortunately, the depth dependence of the hydrate saturation and hence the total volume of hydrate within these hydrate layers is not well constrained. By modeling the physical interactions that control hydrate formation, we can predict the rate of hydrate accumulation and the spatial distribution of the hydrate saturation in different formation environments.

A few issues must be resolved before an accurate quantitative model for the development of marine hydrate layers can be formulated. The first concerns the phase diagram of gas hydrate. The three-phase equilibrium between free gas, hydrate, and aqueous solution has been well studied [e.g., *Sloan*, 1990], but this condition may only apply at the base of hydrate zones in marine sediments. Much less attention has been given to the equilibrium conditions that prevail once temperature and pressure conditions are well within the hydrate stability field. In principle, several combinations of phases may coexist in a two-phase equilibrium within the hydrate stability field, but the most probable phases in a marine setting are hydrate and liquid water (e.g., seawater). Any free gas phase above the base of a marine hydrate layer should be completely incorporated into the hydrate structure as long as excess water is available [*Handa*, 1990], leaving only hydrate and water. Even the residual gas dissolved in the aqueous solution is preferentially incorporated into the hydrate structure as the hydrate becomes more stable. Since most of the hydrate zone lies within the region of two-phase equilibrium, the relationship between pressure, temperature, and dissolved gas concentration in the fluid is an important element of a formation model. It is also essential to understand the importance of crystal growth kinetics [*Englezos et al.*, 1987]. The remote locations of marine hydrate deposits complicate direct observations of the in situ formation conditions and the resulting hydrate layer characteristics. By examining the formation of hydrate layers in less complicated environments we can gain insight into how hydrate growth is controlled by interactions of various physical processes.

In this paper we present quantitative models of hydrate layer formation under conditions which are amenable to testing with laboratory simulations. We begin our discussion with a brief development of the equations that govern the growth and accumulation of a hydrate layer. This sets the stage for a model of hydrate formation in a low-velocity, fluid-saturated, porous medium. We consider the problem of a one-dimensional porous half-space (e.g., $z > 0$) cooled on its lower boundary as an illustrative example and obtain analytical solutions for the hydrate growth. Predictions for the layer growth rate and hydrate saturation are used to show how the hydrate growth depends on the formation conditions. Next, we compare the results of our analytical model with the results of a numerical model that incorporates the nonequilibrium effects of crystal growth kinetics. Nonequilibrium effects are found to be negligible

in natural environments because of the large scale of the problem, but they can be important in laboratory-scale problems. Finally, we quantitatively assess two formation models. One involves advection of gas from below, while the other involves in situ generation of methane within the hydrate zone. These models are discussed in the context of geophysical and geochemical estimates of hydrate saturation in several known occurrences of hydrate.

Governing Equations

We treat the hydrate formation environment as a continuum of sediment grains, fluid, and hydrate crystals. The volume fraction of sediment grains is fixed by the constant porosity ϕ, and the pore space itself is partitioned into solid hydrate with volume fraction h and aqueous solution with volume fraction $1 - h$. As hydrate forms, changes in the relative proportions of hydrate and fluid cause variations in the bulk properties of the continuum. Variations in properties such as heat capacity, bulk density, and thermal diffusivity can effect the evolution of temperature T, pressure P, fluid velocity u, and gas concentration c throughout the porous medium.

Since natural gas concentrations in hydrate-bearing sediments are normally low [*Claypool and Kaplan*, 1974], the liquid-gas mixture is modeled as an incompressible fluid with constant dynamic viscosity η, travelling at velocity u through a fixed, homogeneous porous medium with permeability k. Momentum conservation is described by Darcy's law [e.g., *Phillips*, 1991, p. 27]

$$u = -g(h)\frac{k}{\eta}\nabla P' , \qquad (1)$$

where $\nabla P'$ is the nonhydrostatic pressure gradient and $g(h)$ is a relative permeability function that accounts for the reduction in effective permeability due to clogging of pores with solid hydrate. (The velocity u is often called the transport velocity and it is related to the interstitial velocity v by $u = \phi(1 - h)v$.)

The fluid density ρ_f and hydrate density ρ_h will generally differ; hence the mass balance (see *Rempel* [1994] for details)

$$\rho_f \nabla \cdot u = \phi(\rho_f - \rho_h)\frac{\partial h}{\partial t} , \qquad (2)$$

indicates that the rate of volume change associated with the phase transition induces a divergence of flow. If, however, the density difference and the rate of hydrate production are small, (??) reveals that the flow will be approximately solenoidal (i.e., $\nabla \cdot u \approx 0$).

Heat is transported by advection and dispersion through the fluid and by thermal conduction through the bulk matrix. The bulk thermal conductivity $K(h)$ depends on the hydrate saturation h, so that spatial variations in h can alter the conductive heat flow. Latent heat L is released by the exothermic processes of hydrate forma-

tion, which acts as a heat source in the energy equation. Thus the energy balance can be written as

$$\bar{C}(h)\frac{\partial T}{\partial t} + \mathbf{u} \cdot \nabla T = \nabla \cdot (\kappa(h)\nabla T) + \frac{\rho_h \phi L}{\rho_f C_f}\frac{\partial h}{\partial t} , \quad (3)$$

where the effective thermal diffusivity $\kappa(h)$ (including dispersive effects) and the normalized bulk heat capacity $\bar{C}(h)$ are defined by

$$\kappa(h) \equiv \frac{K(h)}{\rho_f C_f} ,$$

$$\bar{C}(h) \equiv \frac{\rho_f C_f \phi(1-h) + \rho_h C_h \phi h + \rho_s C_s(1-\phi)}{\rho_f C_f} , \quad (4)$$

in which the density ρ and isobaric heat capacity C of the fluid, hydrate, and sediment are represented by the subscripts f, h, and s, respectively.

Gas at a sufficiently low concentration is dissolved or suspended in the pore liquid and transported at velocity $\mathbf{u}$. This advective transport is accompanied by dispersion and diffusion down the compositional gradient. The combined dispersive and diffusive coefficient is denoted by D. (Both dispersion and diffusion are confined to the fluid, so both fluxes have a common dependence on h. This allows us to define a combined diffusive/dispersive coefficient.) It is also possible for the diffusive flux to be driven by gradients in temperature and pressure, although we will not consider these effects further.

Hydrate formation requires a transfer of gas from the fluid into the hydrate. The mass fraction of gas c_h in the hydrate structure is treated as a constant, while the mass fraction c in the fluid is depleted with time as the hydrate grows. Conservation of gas requires

$$(1-h)\frac{\partial c}{\partial t} + \frac{1}{\phi}\mathbf{u} \cdot \nabla c = \nabla \cdot [(1-h)D\nabla c] \quad (5)$$

$$-\frac{\rho_h}{\rho_f}(c_h - c)\frac{\partial h}{\partial t} ,$$

Table 1. Physical Properties

Property	Nominal Value	Units
ρ_f	1000	kg m^{-3}
ρ_h	930	kg m^{-3}
ρ_s	2650	kg m^{-3}
C_f	4200	J kg^{-1} K^{-1}
C_h	2080	J kg^{-1} K^{-1}
C_s	2200	J kg^{-1} K^{-1}
ϕ	0.5	–
L	430	10^3 J kg^{-1}
κ	10^{-7}	m^2 s^{-1}
D	10^{-9}	m^2 s^{-1}

Sources are *Hyndman and Davis* [1992], *Lide* [1990], and *Sloan* [1990].
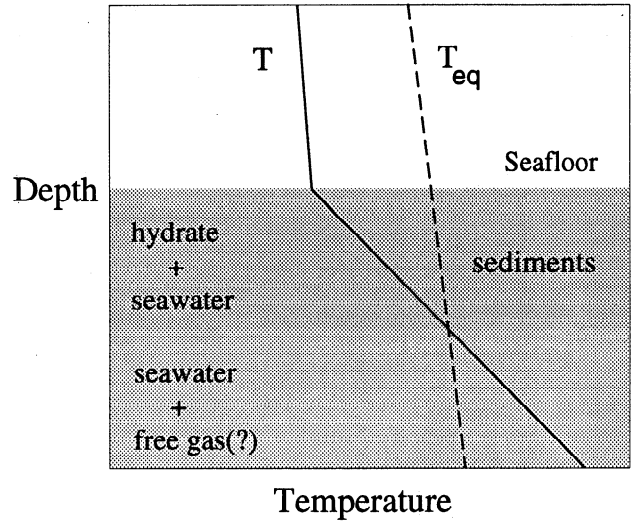

Figure 1. Schematic profile of temperature near the seafloor. The temperature in the deep ocean and shallow seafloor sediments is represented by T. Temperature T_A corresponds to the three-phase equilibrium between gas, hydrate, and liquid water at hydrostatic pressure. Hydrate is stable in the uppermost region of the seafloor sediments where the temperature T falls below T_A. The condition of three-phase equilibrium occurs at the intersection of T and T_A, which defines the base of the hydrate layer.

where the latter term represents a sink of gas due to the incorporation of this gas into the hydrate structure.

Equations (??), (??), (??), and (??), together with the condition of thermodynamic equilibrium, provide a complete description of hydrate formation in uniform porous media. Typical values of the relevant physical parameters are given in Table 1. Numerical techniques may be employed to solve the full nonlinear system; however, we believe that important insights can be gained by retaining only the essential elements of the problem. We use scaling arguments to identify the leading-order terms and obtain a reduced set of equations. We also restrict our attention to solutions which are independent of horizontal coordinates on the grounds that pressure and temperature gradients in marine sediments are predominantly vertical.

Two-Phase Equilibrium

Hydrates in marine environments are typically found in seafloor sediments below water depths of roughly 1000 m, corresponding to a hydrostatic pressure in excess of 10 MPa. The vertical extent of the hydrate layer is limited by a sharp increase in the temperature gradient below the seafloor (see Figure 1). The temperature at the base of the hydrate layer is thought to coincide with the temperature of the three-phase hydrate-gas-liquid equilibrium at hydrostatic pressure. At shallower depths in the hydrate layer, temperatures fall below the three-phase equilibrium value, so only two phases are expected in this region. *Handa* [1990] has noted that

free gas should not be present in a two-phase region as long as water is present in excess; any free gas that might be present should be converted to hydrate using the available water. Thus we expect the sediments throughout most of the hydrate zone to contain solid hydrate and seawater.

Equilibrium calculations for methane hydrate and liquid water [Handa, 1990] indicate that the concentration of gas dissolved in the fluid decreases as the temperature decreases or the pressure increases. In other words, gas is progressively removed from the fluid as the hydrate becomes more stable. Experimental studies using CO_2 hydrate [Yamane and Aya, 1995] support these predictions. A qualitative representation of the gas solubility is indicated in Figure 2 where the mass fraction of dissolved gas is shown as a function of temperature at constant pressure. The break in the curve at A corresponds to the temperature at which hydrate first begins to form when a sufficient supply of gas is available (e.g., the three-phase equilibrium temperature T_A). At higher temperatures the curve represents the usual solubility of a gas-fluid mixture, which decreases slowly with increasing temperature. Temperatures less than T_A correspond to the region where hydrates form. A gas concentration in excess of the values indicated in Figure 2 exists in a free gas phase at high temperature and in the hydrate phase at low temperature.

Several interesting conclusions may be drawn from Figure 2. Consider a closed sample of fluid which is cooled from B. Since the gas concentration is fixed, the sample remains at or below the gas saturation level until the region of hydrate stability is reached. However, hydrate will not be chemically stable at T_A because there
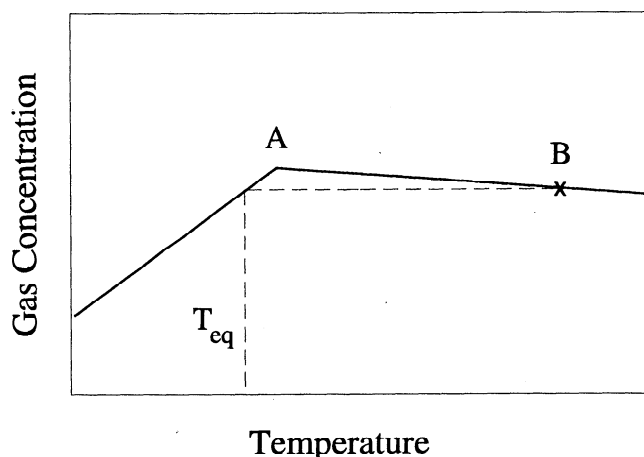

Figure 3. Model calculation involving a homogeneous half-space with porosity ϕ. The boundary is cooled to a temperature T_0 below the hydrate equilibrium temperature T_{eq}. A hydrate layer develops with an advancing interface defined by $z = a(t)$. The hydrate saturation $h(z,t)$ in the layer is a function of both position and time. The initial temperature and gas concentration are denoted by T_∞ and c_∞.

is insufficient dissolved gas. As the sample cools below T_A, hydrate will eventually become stable. We denote this temperature by T_{eq} and emphasize that it falls below T_A because of the low gas concentration in the fluid. Further cooling below T_{eq} promotes hydrate formation, extracting gas from the fluid and decreasing the gas concentration. Hydrate will continue to form until the equilibrium concentration in the fluid is reached. Thus the volume of hydrate produced from an aqueous solution depends on the extent to which the temperature falls below T_{eq}.

In our model calculations we consider the problem of a homogeneous porous half-space saturated with a gas-rich fluid, as depicted in Figure 3. The initial gas concentration c_∞ is at or below the saturation concentration for the initial temperature T_∞. This initial temperature is higher than the equilibrium value T_{eq}. Hydrate begins to form when the lower boundary temperature is dropped below T_{eq} and maintained at T_0. A hydrate layer develops at the boundary and begins to advance into the porous half-space. The equilibrium concentration of gas in the growing hydrate region is assumed to be a linear function of temperature, so that

$$c = c_0 + c'(T - T_0), \qquad T < T_{eq} \qquad (6)$$

where c_0 is the equilibrium concentration at T_0 and c' is a constant inferred from theoretical and experimental

Figure 2. Gas solubility as a function of temperature at constant pressure. A denotes the temperature and dissolved gas concentration at the three-phase equilibrium between hydrate, free gas, and liquid water at the prescribed pressure. When a closed sample of gas-saturated liquid water at B is cooled (path denoted by dashed line), hydrate does not form until the temperature reaches T_{eq}. This temperature is below T_A because the dissolved gas concentration is too low to establish equilibrium at T_A.
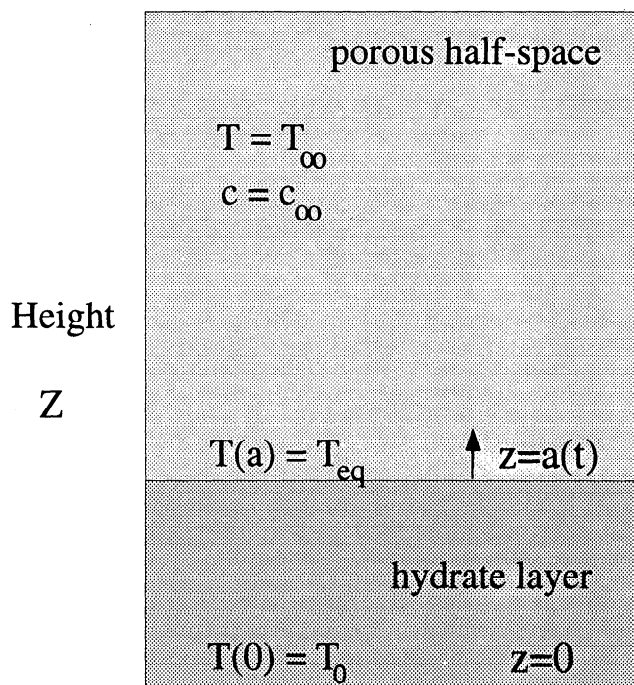
Table 2. Solubility of CH_4 and CO_2

Quantity	CH$_4$	CO$_2$
c_h[a]	1.3×10^{-1}	2.9×10^{-1}
c_∞[b]	1.0×10^{-3}	7.0×10^{-2}
$c'\, K^{-1}$[c]	7×10^{-5}	5×10^{-3}

[a]assumes $CH_4 \cdot 6H_2O$ and $CO_2 \cdot 6H_2O$ for hydrate composition.

[b]CH_4 solubility at 6.06 MPa and 298 K [*Fogg and Gerrard*, 1991]; CO_2 solubility at 30 MPa and 285 K to be consistent with experimental value of c' [*Yamane and Aya*, 1995].

[c]After *Handa* [1990] and *Yamane and Aya* [1995].

studies (see Table 2). This approximation of the two-phase equilibria completes the set of equations needed to model the formation of gas hydrates in porous media.

Dimensionless Equations

To assess the relative importance of advection and diffusion in the governing equations, it is convenient to express the equations in dimensionless form. A suitable length scale for the problem is the thickness of the hydrate layer, which is typically 10^2 m. The thermal diffusion time is

$$\tau = \frac{l^2}{\kappa(0)}, \qquad (7)$$

which is defined in terms of the characteristic length scale $l \approx 10^2$ m and the effective diffusivity $\kappa(h)$ in the absence of hydrate. The corresponding velocity scale for thermal diffusion is

$$u_t = \frac{\kappa(0)}{l}. \qquad (8)$$

It is also convenient to define an effective velocity for chemical diffusion by

$$u_c = \epsilon\, u_t, \qquad (9)$$

where $\epsilon = D/\kappa(0)$ is the ratio of chemical to thermal diffusivity. Both velocity scales are altered slightly by the addition of hydrate, but these changes are not large enough to influence an order of magnitude estimate.

The relative importance of advection and diffusion in (3) and (5) is determined by a comparison of the transport velocity **u** with velocity scales u_t and u_c. When **u** is much less than the diffusive velocity scales, advection can be neglected to leading order in the corresponding conservation equations. Typical thermal conductivities in continental shelf sediments are roughly 10^0 W m^{-1} K^{-1} [*Davis et al.*, 1990] which suggests that $\kappa(h) \approx 10^{-7}$ m^2 s^{-1}. The corresponding velocity scale u_t is 10^{-9} m s^{-1}. Experimental measurements of the chemical diffusivities of light hydrocarbons in sedimentary rocks vary widely, with reported values ranging from 10^{-12} to 10^{-6} m^2 s^{-1} [*Kroos and Leythaeuser*, 1988].

Therefore the velocity scale u_c for chemical diffusion varies from 10^{-14} to 10^{-8} m s^{-1}. By comparison, fluid velocities in the Cascadia accretionary margin, where vast hydrate reserves are located, have been reported with an upper bound of 4×10^{-11} m s^{-1} [*Hyndman et al.*, 1993].

It is clear from the preceding estimates that thermal diffusion dominates the heat transport in most marine environments. The uncertainty in the chemical diffusion coefficient hampers interpretations of the dominant gas transport mechanism. The estimate 4×10^{-11} m s^{-1} falls in the middle of the diffusive estimates inferred from experiments, so it is plausible that fluid flow is primarily responsible for transporting gas in some geographic areas. However, it is also reasonable to expect compositional diffusion to dominate advection at least in some environments. These arguments do not address the possibility of enhanced transport along fractures, but these additional complications are not warranted at this early stage. Since the neglect of advective transport is most suitable for laboratory simulations, we proceed initially on the assumption that chemical diffusion is primarily responsible for gas transport. The effects of fluid transport are subsequently included in a numerical model of hydrate formation.

Dimensionless governing equations are obtained using the thermal diffusion time and by defining suitable scales for temperature and gas concentration. The typical changes in temperature and gas concentration over the hydrate layer are $T_\infty - T_0$ and $c_\infty - c_0$, so we define dimensionless temperature and gas concentrations by

$$\tilde{T} \equiv \frac{T - T_0}{T_\infty - T_0},$$

$$\tilde{c} \equiv \frac{c - c_0}{c_\infty - c_0}. \qquad (10)$$

On introducing these dimensionless quantities and eliminating the advective transport, the energy and gas conservation equations reduce to

$$\bar{C}(h)\frac{\partial \tilde{T}}{\partial \tilde{t}} = \frac{\partial}{\partial \tilde{z}}\left(\frac{\kappa(h)}{\kappa(0)}\frac{\partial \tilde{T}}{\partial \tilde{z}}\right) + S\,\frac{\partial h}{\partial \tilde{t}}, \qquad (11)$$

$$(1-h)\frac{\partial \tilde{c}}{\partial \tilde{t}} = \epsilon\frac{\partial}{\partial \tilde{z}}\left((1-h)\frac{\partial \tilde{c}}{\partial \tilde{z}}\right) - \frac{\rho_h}{\rho_f}(\tilde{c}_h - \tilde{c})\,\frac{\partial h}{\partial \tilde{t}}, \qquad (12)$$

where $\tilde{t}$ and $\tilde{z}$ are the dimensionless counterparts to t and z, while S, ϵ, and $\tilde{c}_h$ are defined by

$$S \equiv \frac{\rho_h \phi L}{\rho_f C_f (T_\infty - T_0)},$$

$$\epsilon \equiv \frac{D}{\kappa(0)},$$

$$\tilde{c}_h \equiv \frac{c_h - c_0}{c_\infty - c_0}. \qquad (13)$$

The Stefan number S measures the importance of the latent heat release relative to the heat required to change

the temperature of the porous medium. The Lewis number ϵ indicates the relative efficiency of heat and gas diffusion, while the concentration $\tilde{c}_h$ is a dimensionless measure of the amount of gas contained in the hydrate structure. The two-phase equilibria, defined by (6), can be written in dimensionless form as

$$\tilde{c} = \tilde{c}'\tilde{T} \qquad \tilde{T} < \tilde{T}_{eq} \qquad (14)$$

where the dimensionless constant is given by $\tilde{c}' = c' \times (T_\infty - T_0)/(c_\infty - c_0)$. Since the far-field concentration c_∞ (say, point B in Figure 2) is equal to the concentration at T_{eq}, it follows from our scaling convention that $\tilde{c}' = \tilde{T}_{eq}^{-1}$.

An Equilibrium Model

When kinetic barriers to crystal growth are small compared with other rate-limiting processes, it is convenient to assume that the hydrate is in thermodynamic equilibrium with the surrounding fluid. The validity of this approximation depends on the timescales that characterize the other processes. Once hydrate crystals begin to nucleate, their continued growth depends on the supply of gas and the removal of latent heat. Thus the kinetics of crystal growth may be safely neglected if the growth time associated with nonequilibrium effects is much shorter than both the thermal and chemical diffusion times.

Empirical models for nonequilibrium crystal growth typically relate the growth rate to some measure of the disequilibrium. A common measure of the disequilibrium is the amount of dissolved gas in excess of the equilibrium concentration, as given by (6). For a first-order model, the rate of consumption of gas can be described by

$$\frac{dc}{dt} = -\mathcal{K}(c - c_{eq}), \qquad (15)$$

where c_{eq} is the equilibrium value defined in (6) and $\mathcal{K}$ is the reaction rate constant. More deterministic models for the nonequilibrium effects [Englezos et al., 1987] yield qualitatively similar results, although $\mathcal{K}$ is not strictly a constant. However, experiments on methane hydrate formation suggest that $\mathcal{K} \approx 10^{-3}$ s^{-1} (T. Uchida, personal communication, 1996) over a range of pressure and temperature conditions, so the characteristic formation time $\mathcal{K}^{-1}$ is much shorter than 10^{11} s, which is a typical time for thermal diffusion in marine environments. While nonequilibrium effects are expected to be negligible in natural environments, they are liable to be more important in laboratory experiments where physical dimensions are much smaller.

The assumption of thermodynamic equilibrium implies that the temperature and gas concentration in the hydrate zone are related by (14). Pressure varies slightly across the hydrate layer, but the equilibrium temperature and gas concentration vary slowly with pressure. Consequently, we may safely assume that the parameter $\tilde{c}'$ in (14) remains constant over the entire hydrate layer. We assume in our calculations that the hydrate layer grows from the cooled boundary at $\tilde{z} = 0$ and that the advancing hydrate interface is defined by $\tilde{z} = a(\tilde{t})$. Inside the hydrate layer, $\tilde{T}$ and $\tilde{c}$ obey (11) and (12), but the condition of thermodynamic equilibrium (14) imposes a strong constraint which we exploit to obtain solutions.

The gas concentration in the hydrate layer is altered by the combined effects of diffusion and hydrate formation. The relative importance of diffusion in (12) depends on the Lewis number ϵ. For typical parameter values, $\epsilon \ll 1$, so (12) is primarily a balance between the depletion of gas in the fluid and the local consumption of gas due to hydrate formation. An approximate gas balance may be expressed as

$$(1 - h)\frac{\partial \tilde{c}}{\partial \tilde{t}} = -\frac{\rho_h}{\rho_f}(\tilde{c}_h - \tilde{c})\frac{\partial h}{\partial \tilde{t}}, \qquad (16)$$

which can be integrated directly to give

$$(1 - h)^{\rho_h/\rho_f} = \left(\frac{\tilde{c}_h - 1}{\tilde{c}_h - \tilde{c}}\right). \qquad (17)$$

Simpler approximations for h are possible because $\rho_h/\rho_f \approx 1$ and $\tilde{c} \ll \tilde{c}_h$ (e.g., large storage of gas in hydrate structure). Invoking these simplifications yields

$$h(\tilde{z}, \tilde{t}) \approx \left(\frac{1 - \tilde{c}}{\tilde{c}_h}\right), \qquad (18)$$

which provides a reliable estimate of the hydrate saturation. The accuracy of this estimate is confirmed by subsequent comparisons with a complete numerical solution.

The energy equation (11) in the hydrate layer may now be expressed solely in terms of $\tilde{T}$ by eliminating h using (18) and $\tilde{c}$ using the thermodynamic relation (14). The resulting equation for $\tilde{T}$ in $0 < \tilde{z} < a(\tilde{t})$ is

$$\left(\mathcal{C}(\tilde{T}) + \mathcal{S}\right)\frac{\partial \tilde{T}}{\partial \tilde{t}} = \frac{\partial}{\partial \tilde{z}}\left(\frac{\kappa(\tilde{T})}{\kappa}\frac{\partial \tilde{T}}{\partial \tilde{z}}\right), \qquad (19)$$

where

$$\mathcal{S} = S\,\tilde{c}'\,\tilde{c}_h^{-1}$$

$$\mathcal{C}(\tilde{T}) = \bar{C}(0) + \Delta\bar{C}(1 - \tilde{c}'\tilde{T}), \qquad (20)$$

$$\Delta\bar{C} = \frac{\phi}{\tilde{c}_h}\left(\frac{\rho_h C_h - \rho_f C_f}{\rho_f C_f}\right),$$

and $\bar{C}(0)$ is the usual bulk heat capacity defined by (4) when $h = 0$. We use $\mathcal{C}(\tilde{T})$ to denote the same bulk heat capacity when it is expressed as a function of temperature. The diffusivity $\kappa(\tilde{T})$ is also dependent on temperature through its dependence on h. However, the thermal conductivity of water is remarkably similar to that for hydrate. It follows that the thermal diffusivity,

as defined by (4), remains nearly constant as hydrate forms. Under these circumstances it is reasonable to set $\kappa(\tilde{T})/\kappa = 1$. Unfortunately, it is not possible to introduce a similar simplification for the heat capacity $\mathcal{C}(\tilde{T})$ because C_f is approximately twice as large as C_h.

Manipulations leading to (19) have a straightforward interpretation. The latent heat release, which appeared explicitly in (11), is now included as the contribution $\mathcal{S}$ to the specific heat. In this form we view the latent heat as an anomaly in the specific heat. We also note that the temperature dependence of $\mathcal{C}(T)$ reflects a change in bulk properties due to hydrate formation. The amplitude of this temperature dependence is proportional to $\Delta\bar{C}$, which includes in its definition the difference in heat capacities $\rho_f C_f - \rho_h C_h$ and the volume of hydrate present (roughly proportional to $\tilde{c}_h^{-1}$). Once a solution to (19) is obtained for temperature in the hydrate layer, estimates for $\tilde{c}$ and $\tilde{h}$ are given by (14) and (18).

Although the distribution of $\tilde{c}$ and $\tilde{h}$ through the hydrate layer is unknown prior to solving for the temperature $\tilde{T}$, the values at the boundaries of the hydrate layer are known from the boundary conditions. The imposed dimensionless temperature at $\tilde{z} = 0$ is

$$\tilde{T}(0, \tilde{t}) = 0 \qquad (21)$$

which implies that $\tilde{c} = 0$ and $h = \tilde{c}_h^{-1}$ by the assumptions of thermodynamic equilibrium and small Lewis number. At the top of the hydrate layer, $\tilde{z} = a(\tilde{t})$, the hydrate saturation vanishes, the gas concentration equals the initial value $\tilde{c} = 1$, and

$$\tilde{T}(a, \tilde{t}) = \tilde{T}_{eq} . \qquad (22)$$

Since the hydrate saturation vanishes at the top of the hydrate layer there is no discontinuity in h across the interface $\tilde{z} = a(\tilde{t})$. (This absence of an abrupt hydrate front distinguishes the present problem from some previous studies of hydrate dissociation [*Selim and Sloan*, 1989; *Tsypkin*, 1991].) It follows from conservation of energy that the temperature gradient across the interface is continuous. Solutions for the temperature outside the hydrate layer are obtained by solving (11) with $h = 0$. These solutions are subject to continuity conditions on $\tilde{T}$ and $d\tilde{T}/d\tilde{z}$ at $\tilde{z} = a(\tilde{t})$, and the far-field condition $\tilde{T} = 1$ as $\tilde{z} \to \infty$.

Similarity Solution

Solutions for $\tilde{T}$ throughout the porous medium are conveniently found in terms of a similarity variable

$$\xi \equiv \frac{\tilde{z}}{2\sqrt{\tilde{t}}} . \qquad (23)$$

It is also convenient to express the interface position in the form

$$a(\tilde{t}) = 2\lambda\sqrt{\tilde{t}} , \qquad (24)$$

so that the interface position, defined in terms of the

similarity variable, becomes $\xi = \lambda$. Expressing the energy equation (19) in terms of ξ yields

$$\frac{d^2\tilde{T}}{d\xi^2} + 2\xi\left(\mathcal{C}(\tilde{T}) + \mathcal{S}\right)\frac{d\tilde{T}}{d\xi} = 0, \quad 0 < \xi < \lambda \qquad (25)$$

inside the hydrate layer. The energy equation outside the hydrate layer is given by (11) after setting $h = 0$. Introducing the similarity variable ξ yields

$$\frac{d^2\tilde{T}}{d\xi^2} + 2\xi\bar{C}(0)\frac{d\tilde{T}}{d\xi} = 0, \quad \lambda < \xi < \infty \qquad (26)$$

The boundary conditions on $\tilde{T}(\xi)$ become

$$\tilde{T}(0) = 0$$

$$\tilde{T}(\lambda) = \tilde{T}_{eq} \qquad (27)$$

$$\tilde{T}(\infty) = 1$$

in addition to the continuity condition on $d\tilde{T}/d\tilde{z}$ at $\xi = \lambda$. In fact, it is this condition on the continuity of the gradient which is used to evaluate the constant λ.

Integrating (26) for the temperature outside of the hydrate layer ($\lambda < \xi < \infty$) gives

$$\tilde{T}(\xi) = \text{erf}\left(\xi\sqrt{\bar{C}(0)}\right) + \frac{\tilde{T}_{eq} - \text{erf}(\lambda\sqrt{\bar{C}(0)})}{\text{erfc}(\lambda\sqrt{\bar{C}(0)})} \qquad (28)$$

$$\times \, \text{erfc}\left(\xi\sqrt{\bar{C}(0)}\right) ,$$

where $\text{erf}(x)$ is the error function and $\text{erfc}(x)$ is the complementary error function [*Abramowitz and Stegun*, 1972]. Unfortunately, a direct integration of (25) for the temperature inside the hydrate layer is not as straightforward because the equation is nonlinear. However, the nonlinearity is weak because typical variations in $\mathcal{C}(\tilde{T})$ with temperature are small. Consequently, it is possible to obtain solutions to (25) using perturbation methods.

A first approximation to (25) can be found by replacing the specific heat $\mathcal{C}(\tilde{T})$ with $\mathcal{C}(0)$. When deviations between $\mathcal{C}(\tilde{T})$ and $\mathcal{C}(0)$ are small, the resulting equation provides a reasonable approximation to (25). Such an approximation is justified when the hydrate saturation is small or, equivalently, when $\Delta\bar{C} \ll \bar{C}(0)$. The approximate solution $\tilde{T}^0$ that satisfies the temperature boundary conditions at $\xi = 0$ and λ is

$$\tilde{T}^0(\xi) = \tilde{T}_{eq}\frac{\text{erf}(\xi\sqrt{\mathcal{C}(0) + \mathcal{S}})}{\text{erf}(\lambda\sqrt{\mathcal{C}(0) + \mathcal{S}})} , \quad 0 < \xi < \lambda \qquad (29)$$

A second, improved approximation is obtained by using $\tilde{T}^0$ to evaluate $\mathcal{C}(\tilde{T})$. On replacing $\mathcal{C}(\tilde{T})$ in (25) with $\mathcal{C}(\tilde{T}^0)$ we get a more accurate governing equation which can be readily integrated. Integrating once with respect to ξ gives

$$\ln \frac{d\tilde{T}}{d\xi}\bigg|_0^\xi = -2 \int_0^\xi x\left(\mathcal{C}(0) + \mathcal{S}\right) dx \qquad (30)$$

$$+ 2\tilde{c}' \Delta\bar{C} \, \tilde{T}_{eq} \int_0^\xi \frac{\text{erf}(x\sqrt{\mathcal{C}(0)+\mathcal{S}})}{\text{erf}(\lambda\sqrt{\mathcal{C}(0)+\mathcal{S}})} \, dx \,,$$

although, for practical purposes, it suffices to approximate the error functions using

$$\frac{\text{erf}(x\sqrt{\mathcal{C}(0)+\mathcal{S}})}{\text{erf}(\lambda\sqrt{\mathcal{C}(0)+\mathcal{S}})} \approx \frac{x}{\lambda}. \qquad (31)$$

A second integration with respect to ξ gives the temperature inside the hydrate layer,

$$\tilde{T}(\xi) = \tilde{T}_{eq}\frac{F(\xi)}{F(\lambda)}, \qquad (32)$$

where

$$F(\xi) = \int_0^\xi e^{-x^2(\mathcal{C}(0)+\mathcal{S}-x\Delta\mathcal{C})} dx \qquad (33)$$

and

$$\Delta\mathcal{C} = \frac{2}{3}\left(\frac{\tilde{T}_{eq}\tilde{c}'}{\lambda}\right)\Delta\bar{C}. \qquad (34)$$

The function $F(\xi)$ may be evaluated numerically, although we note that F reduces to the form of an error function when $\Delta\mathcal{C}$ vanishes. Hence, in the special case when $\Delta\mathcal{C} \approx 0$, the solution for $\tilde{T}$ reduces to that given in (29).
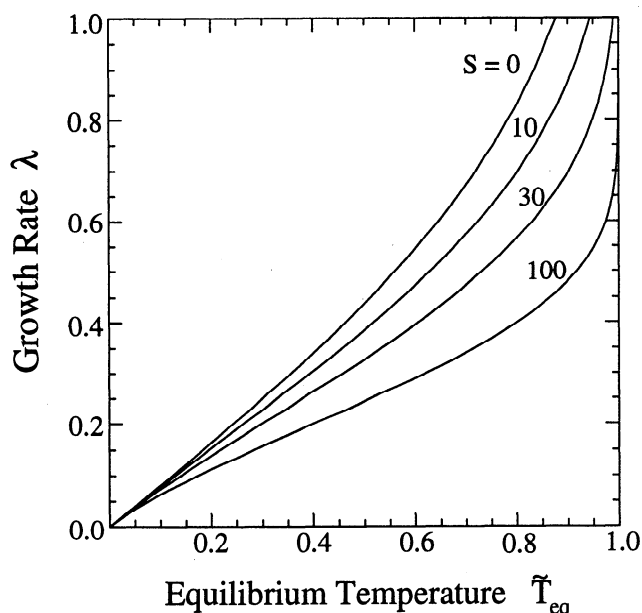
Figure 4. The dependence of the growth rate λ on the dimensionless equilibrium temperature $\tilde{T}_{eq} = (T_{eq} - T_0)/(T_\infty - T_0)$. Several results are obtained using different values of the Stefan number S. The growth rate increases with $\tilde{T}_{eq}$ to the limiting case $\tilde{T}_{eq} = 1$, where the far-field temperature is equal to the formation temperature. Hydrate formation in this case is limited by latent heat removal, and consequently, the effect of varying S is more pronounced.

Table 3. Dimensionless Parameters

Parameter	CH$_4$	CO$_2$
$\bar{C}(0)$	1.2	1.2
$\Delta\bar{C}$	-0.001	-0.03
S	0.3	10
$\mathcal{S}$	0.03	1.0
ϵ	0.01	0.01
$\tilde{c}_h$	360	9.8

Concentration scales $c_\infty - c_0$ are calculated using theoretical values of c' and a typical temperature variation $T_\infty - T_0 = 5$ K.

The final step in the calculation is to evaluate the interface position λ from the condition that the temperature gradients on either side of the hydrate interface are continuous. Matching the gradients of the solutions given in (28) and (32) requires

$$2\sqrt{\frac{\bar{C}(0)}{\pi}}\frac{(1-\tilde{T}_{eq})}{\text{erfc}(\lambda\sqrt{\bar{C}(0)})}e^{-\lambda^2\bar{C}(0)} \qquad (35)$$

$$-\frac{\tilde{T}_{eq}}{F(\lambda)}e^{-\lambda^2(\mathcal{C}(0)+\mathcal{S}-\lambda\Delta\mathcal{C})} = 0$$

which defines a transendental equation for λ. Once the value of λ is found numerically using a Newton-Raphson method, solutions for $\tilde{T}$ are given by (28) and (32). The values of $\tilde{c}$ and h inside the hydrate layer are given by (14) and (18), completing the calculation.

Predictions of the Equilibrium Model

The position of the interface, $\tilde{z} = a(\tilde{t})$, is defined in terms of λ by (24). Higher values of λ correspond to more rapid hydrate growth, so it is convenient to view λ as a measure of the growth rate. The value of λ that solves (35) is dependent on the values of a number of dimensionless parameters. These parameters are, in turn, functions of the prescribed pressure and temperature conditions, as well as the chemistry of the hydrate-aqueous solution system. Given the physical constraints posed by the chemistry of the system, it is evident that the two most important variables which can be altered to control model behavior are the degree of undercooling, represented by the dimensionless equilibrium temperature $\tilde{T}_{eq}$, and the latent heat release which is measured by the Stefan number S. Representative model parameters for both methane hydrate and carbon dioxide hydrate are given in Table 3. These parameters are used to solve (35) and show the dependence of model behavior on the values of S and $\tilde{T}_{eq}$.

Figure 4 uses the CO$_2$ hydrate formation parameters listed in Table 3 to illustrate the dependence of the growth rate λ on $\tilde{T}_{eq}$. Each solid line represents this relationship at a different value of the Stefan number S. When the degree of undercooling is low at small $\tilde{T}_{eq}$,

layer growth is rate-limited by the process of cooling the aqueous solution to the hydrate equilibrium temperature. The Stefan number is less important in this regime because the heat associated with cooling dominates the latent heat in the heat budget. As a result, the four curves coincide when $\tilde{T}_{eq}$ goes to 0. As $\tilde{T}_{eq}$ is increased (e.g., the initial temperature is closer to the equilibrium temperature), less heat must be removed to cause hydrate formation and the layer grows more rapidly. The growth rate is increasingly dependent on the Stefan number S at higher degrees of undercooling. In fact, when $\tilde{T}_{eq}$ approaches unity, the growth of the layer is retarded only by the need to remove latent heat since the initial solution temperature is already at the equilibrium temperature. For comparison, we note that the model describes the cooling of a half-space when $S = 0$.

The four curves in Figure 5 show the growth rate λ as a function of the Stefan number S at different degrees of undercooling $\tilde{T}_{eq}$. As S tends to zero, λ is determined by the rate at which the aqueous solution can be cooled. When S is increased, the need to remove more latent heat slows the rate of cooling and layer growth is slowed. When the degree of undercooling is greater at higher values of $\tilde{T}_{eq}$ the importance of latent heat removal and hence the dependence of λ on the Stefan number is more pronounced.

Figure 5. The dependence of growth rate λ on the Stefan number S, as defined by (13), which measures the importance of latent heat release. Several results are obtained using different values of the equilibrium temperature $\tilde{T}_{eq}$. In all cases the growth rate decreases with increasing S because the increasing effects of latent heat release slow the rate of cooling.

A Numerical Model

A numerical implementation of the full governing equations (1)–(5) serves a number of useful purposes. First, it is possible to assess the validity of the approximations used in our equilibrium model. Second, we can assess the role of nonequilibrium effects, which are liable to be important in laboratory-scale problems. Finally, we can extend the calculations to situations that are more representative of the formation conditions in natural environments. The numerical calculations presented here are limited to one spatial dimension, but no further restrictions are imposed on the solutions. In this case the solutions are readily obtained using the method of lines [Sincovec and Madsen, 1978].

The nonequilibrium effects are modelled using an empirical first-order equation of the form given in (15). When this kinetic model is expressed in dimensionless form, the reaction rate constant is defined in terms of the thermal diffusion time. Thus a value $\mathcal{K} = 1$ implies that the effects of phase kinetics and thermal diffusion have comparable time scales, whereas larger values of $\mathcal{K}$ indicate that kinetic effects are more rapid than thermal diffusion. Calculations for several different values of $\mathcal{K}$ are obtained for the problem of a porous half-space cooled on its boundary. The results of these calculations for large $\mathcal{K}$ may be compared directly with the results of the equilibrium model to assess the accuracy of that model.

The numerical solution for temperature is found to agree well with the prediction of the equilibrium model,
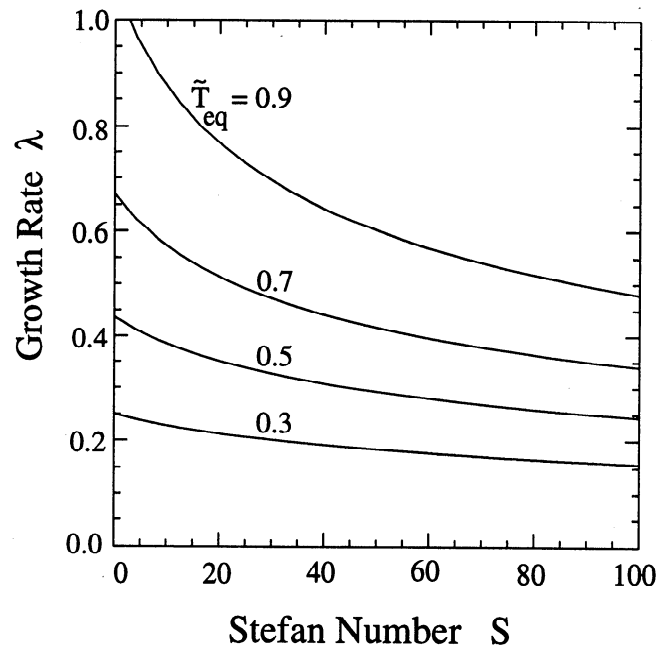
but such a comparision does not reveal some of the subtle differences between the two solutions. We focus instead on the results for gas concentration and hydrate saturation. A comparison of the solutions for gas concentration as a function of position from the cooled boundary is shown in Figure 6. The analytical (equilibrium) solution is indicated by the dashed line, while the numerical solutions obtained with different values of $\mathcal{K}$ are indicated by solid lines. Hydrate begins to form in the region nearest the boundary as the porous half-space is cooled. Gas is extracted from the fluid as the hydrate forms, lowering the dimensionless gas concentration $\tilde{c}$ from the far-field value $\tilde{c}_{\infty} = 1$. In the equilibrium model the gas concentration is immediately reduced to the equilibrium value predicted by (14). By contrast, a smaller reduction occurs in the numerical model, depending on the value of $\mathcal{K}$. However, once $\mathcal{K} = 100$, the differences between the numerical and equilibrium model are small. The largest difference occurs at the leading edge of the hydrate front (roughly $\tilde{z} = 0.15$), where there has been insufficient time to relax into an equilibrium state, and at the boundary $\tilde{z} = 0$, where a no flux condition (e.g., $d\tilde{c}/d\tilde{z} = 0$) is imposed on the numerical solution.

A complementary picture emerges from a comparison of the predicted hydrate saturation h, as shown in Figure 7. The largest hydrate saturation occurs where the reduction in the gas concentration is greatest, and this always occurs at the boundary $\tilde{z} = 0$. In the equi-
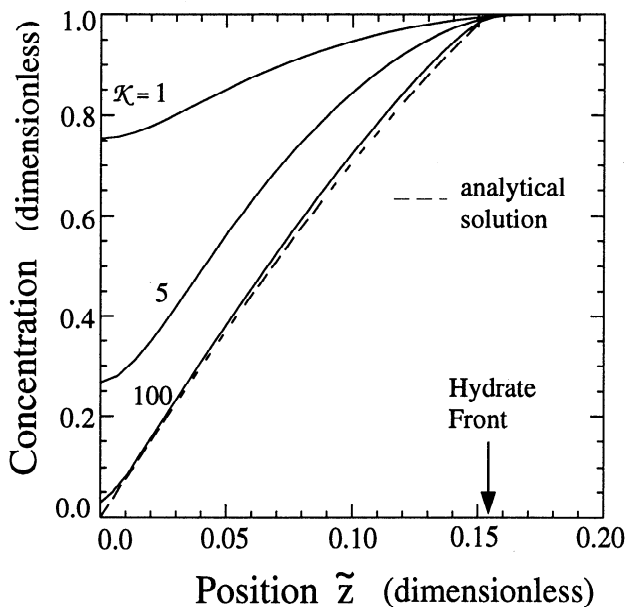
Figure 6. Numerical solution for the dimensionless gas concentration in a porous medium which is cooled on its boundary ($\tilde{z} = 0$). Solutions are obtained using three different values of the reaction rate constant $\mathcal{K}$, and the results are compared with the analytical (equilibrium) model. The leading edge of the growing hydrate zone is located near $\tilde{z} = 0.15$.

librium model the hydrate saturation decreases almost linearly across the hydrate zone. Smaller hydrate saturations develop when the phase change is limited by kinetic effects, but the value $\mathcal{K} = 100$ once again yields results which are in reasonably good agreement with the analytical solution. One exception occurs at the boundary $\tilde{z} = 0$ where the hydrate saturation predicted by the numerical solution ($\mathcal{K} = 100$) actually exceeds the equilibrium prediction. These difference can be attributed, in part, to the effects of chemical diffusion, which are neglected in our equilibrium model. Chemical diffusion can be important at early times when the gradients in gas concentration are very steep. In fact, the gradient in gas concentration is infinite at the boundary in the equilibrium model when $\tilde{t} = 0$. Diffusion of gas into the thin hydrate zone that develops at early times can elevate the hydrate saturation, as indicated in Figure 7. As the hydrate layer becomes thicker with time and the chemical gradient becomes smaller, the diffusive transport of gas is reduced, and the two solutions are once again in good agreement.

The good agreement between the equilibrium model and the numerical predictions for large $\mathcal{K}$ indicates that the approximations used in the equilibrium model are reasonable. The importance of kinetic effects is seen to depend on the dimensionless value of $\mathcal{K}$, which is expressed in terms of a thermal diffusion timescale. Therefore the role of kinetics will depend on the physical dimensions of the problem of interest. In the marine environment, where a typical length scale is 100 m, the dimensionless value of $\mathcal{K}$ is approximately 10^8. Conse-

quently, kinetic effects are very fast compared with thermal diffusion, and the equilibrium approximation may be safely assumed. In laboratory experiments, where a typical physical dimension might be 0.1 m or less, the dimensionless value of $\mathcal{K}$ is 100 or less. Thus kinetic effects are liable to be more important in laboratory studies.

Application to Marine Environment

There are competing conceptual models for the formation of hydrate in marine sediments. One model favors generation of methane by biogenic activity within the hydrate zone [*Kvenvolden and Barnard*, 1983; *Brooks et al.*, 1985], while the other model argues for a flux of methane into the hydrate zone from below [*Hyndman and Davis*, 1992; *Paull*, 1994]. The one-dimensional numerical solutions described in the preceding section can be adapted to quantitatively assess both of these models.

We begin with the situation where methane is fluxed into the hydrate zone from below by the combined effects of vertical advection and diffusion. We assume that a reservoir of gas exists below the hydrate zone where the concentration of gas dissolved in the fluid is roughly constant (see Figure 8). Free gas may exist below the hydrate zone, but we assume that this free gas is not transported into the hydrate zone by fluid motion. Instead, the free gas maintains the concentration of gas dissolved in the fluid beneath the hydrate zone at a nearly fixed (saturated) value. For simplicity, we
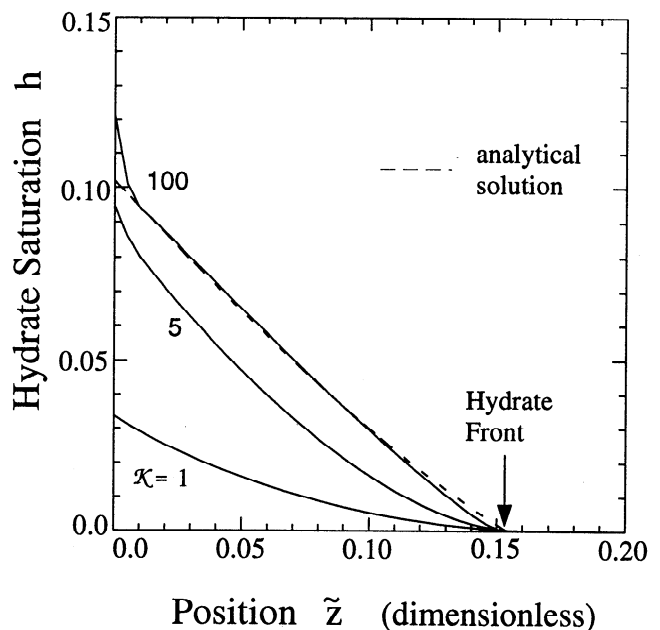

Figure 7. Numerical solution for the hydrate saturation in a porous medium which is cooled on its boundary ($\tilde{z} = 0$). Solutions are obtained using three different values of the reaction rate constant $\mathcal{K}$, and the results are compared with the analytical (equilibrium) model.

z = 100 m   seafloor

Height

Z

$c_{eq}(P,T)$

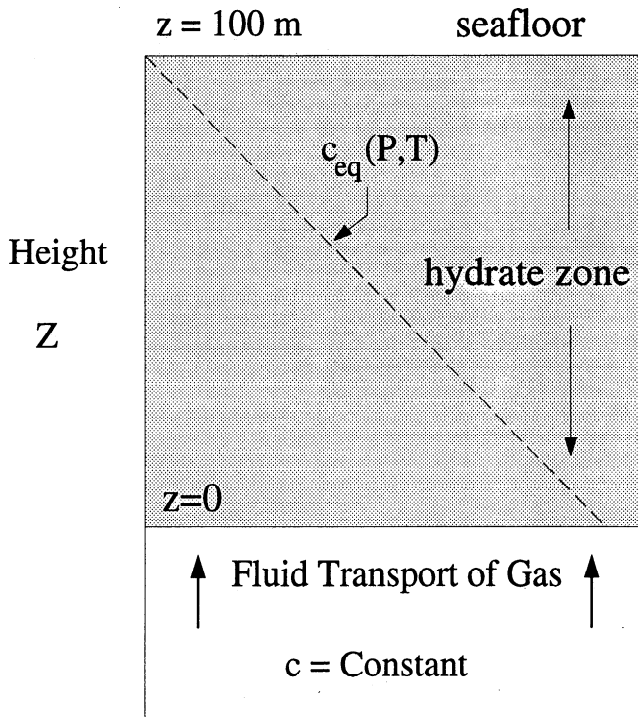hydrate zone

z=0

↑ Fluid Transport of Gas ↑

c = Constant

Figure 8. Schematic profile of marine sediments near the seafloor. A supply of methane gas is dissolved in seawater below the hydrate zone. This dissolved gas is transported into the hydrate zone by the combined effects of advection and diffusion. The equilibrium concentration c_{eq} is defined by the two-phase equilibrium between hydrate and seawater, and it decreases across the hydrate zone.

tion inside the hydrate layer. (The layer thickness is used as the characteristic length scale, and the change in the equilibrium concentration across the layer is used to scale the gas concentration.) Profiles of gas concentration at times $\tilde{t} = 0.5$, 1.0, and 2.0 (in thermal diffusion time) show a progressive intrusion of gas into the hydrate zone. The gas concentrations do not exceed the equilibrium concentration because any excess gas is removed from the fluid by hydrate formation. During this transient part of the calculation a small amount of hydrate accumulates at the base of the hydrate layer wherever the profile has reached the equilibrium concentration. At later times the profile of gas concentration reaches the equilibrium concentration everywhere within the hydrate layer and hydrate forms throughout the layer.

A very simple expression for the rate of hydrate formation can be obtained once the gas concentration reaches the steady, equilibrium profile. When the effects of diffusive gas transport are small compared with the advective transport, the equation for gas conservation reduces to

$$\frac{\partial h}{\partial t} = -\frac{\rho_f \mathbf{u} \cdot \nabla c_{eq}}{\rho_h \phi (c_h - c_{eq})} \qquad (36)$$

when $c = c_{eq}$ in the hydrate zone. This expression for the rate of hydrate formation is dependent on depth, so it can be integrated to predict the vertical distribution of hydrate saturation. Since the factor $c_h - c_{eq}$ is nearly constant, the depth dependence is determined mainly by the term $\mathbf{u} \cdot \nabla c_{eq}$. In our calculations we have
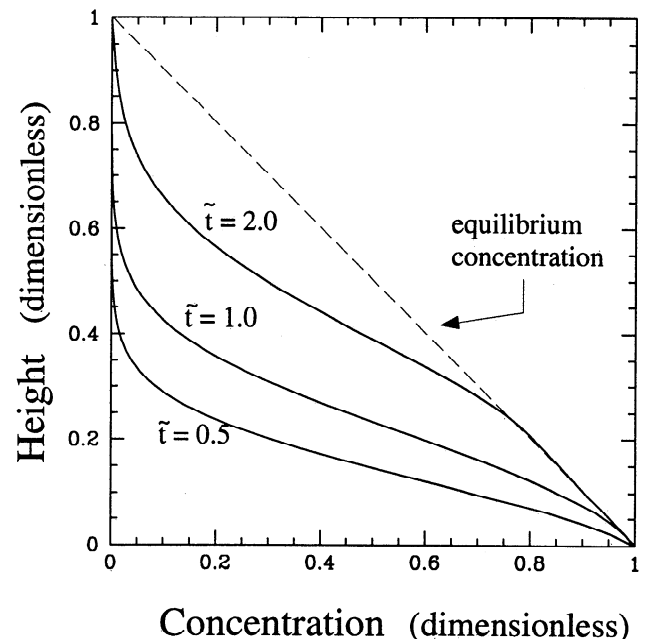
assume that the concentration of dissolved gas beneath the hydrate layer is everywhere equal to the equilibrium value $c_{eq}(P,T)$ at the base of the hydrate layer, which represents the gas saturation at these P and T conditions. The equilibrium concentration decreases with height through the hydrate layer because the pressure and temperature conditions increasingly promote hydrate formation.

The heat transported vertically by fluid advection represents a small perturbation on the large-scale diffusive heat transport in most marine environments. Consequently, we impose boundary conditions on temperature at the top and bottom of the hydrate layer assuming a temperature gradient of 0.05 K m^{-1}. We also impose boundary conditions on the concentration of gas dissolved in the fluid. The value at the top boundary is taken to represent seawater, while the bottom boundary is fixed by the gas reservoir below the hydrate zone. As an initial value, we set the gas concentration through the interior of the hydrate layer equal to the seawater value. The combined effects of advection and diffusion carry gas into the hydrate layer and cause hydrates to form once the gas concentration exceeds the equilibrium value c_{eq}.

Figure 9 shows the evolution of the dimensionless gas concentration as a function of the dimensionless posi-

Concentration (dimensionless)

Figure 9. Evolution of the dissolved gas concentration in the hydrate zone due to advection and diffusion of gas from below. Increases in gas concentration are limited by the equilibrium concentration since any excess gas is removed from the fluid by hydrate formation. A steady state profile eventually develops in which the gas concentration coincides with the equilibrium profile.

assume that both u and ∇c_{eq} are constant, so it follows that $\partial h/\partial t$ is also constant within the layer. However, theoretical phase-equilibrium calculations by O. Zatsepina and B. A. Buffett (Chemical equilibrium of gas hydrates: Implications for the formation of hydrate in the deep seafloor, submitted to Geophysical Research Letters, 1997) have shown that $|\nabla c_{eq}|$ is largest at the base of the hydrate, which implies that the hydrates will form more rapidly at the base of the layer. The predicted increase in hydrate saturation over the lowermost 80–100 m of the hydrate layer is consistent with both geophysical and geochemical estimates [Rowe and Gettrust, 1993; Singh and Minshull, 1994; Yuan et al., 1996]. For illustrative purposes, we assume a vertical velocity of 4×10^{-11} m s^{-1} and find that the typical additive increase in the hydrate saturation is 1% of the pore volume in roughly 10^5 years.

The second model for hydrate formation involves biogenic generation of methane inside the hydrate layer. If methane production is roughly uniform through the layer, then we would expect hydrate to first appear near the top of the layer because the equilibrium concentration is lowest there. Continued methane production would eventually elevate the concentration everywhere in the layer to the equilibrium value and hydrate would form throughout the layer. The vertical distribution of hydrate would be fairly uniform or even concentrated toward the seafloor if chemical diffusion of gas is significant. Such a distribution is inconsistent with some indirect observations which suggest that hydrate saturation increases with depth. This inconsistancy can be reconciled by allowing some alteration of conditions in the sediments. For example, continued sedimentation will shift the geotherm because the newly deposited sediments are maintained at the constant seafloor temperature. As the buried sediments begin to experience a temperature increase, hydrate at the base of the zone will dissociate. The released methane will migrate back into the hydrate zone in a recycling process that could concentrate hydrate at the base of the layer.

If we start with a uniform hydrate saturation of 1%, then the redistribution of hydrate that accompanies a gradual warming of the marine sediments due to burial is shown in Figure 10. Assuming a burial rate of 1 mm yr^{-1} and a geotherm of 0.05 K m^{-1}, we allow the temperature on the top and bottom boundaries to increase at 5×10^{-5} K yr^{-1}. The gas concentration on the top boundary is maintained at the seawater value, while a no flux condition (e.g. $d\tilde{c}/d\tilde{z} = 0$) is imposed on the lower boundary to prevent gas from escaping out the bottom.

After a period of time (roughly 6000 years in dimensional units), the base of the hydrate has moved from its initial position at $\tilde{z} = 0$ to $\tilde{z} = 0.2$. Most of the hydrate in this region has dissociated, causing an increase in the gas concentration. A small amount of hydrate remains below the hydrate zone because the dissociation is weakly limited by kinetic effects. All of the gas

in excess of $\tilde{c} = 1$ would be expected to be present as free gas. This excess gas migrates back into the hydrate zone, but the tranport is slow if it occurs entirely by chemical diffusion. As a result, hydrate formation tends to be concentrated near the base of the hydrate zone. The width of the peak in the hydrate saturation is determined primarily by the effects of latent heat release and phase-change kinetics. When gas is diffused
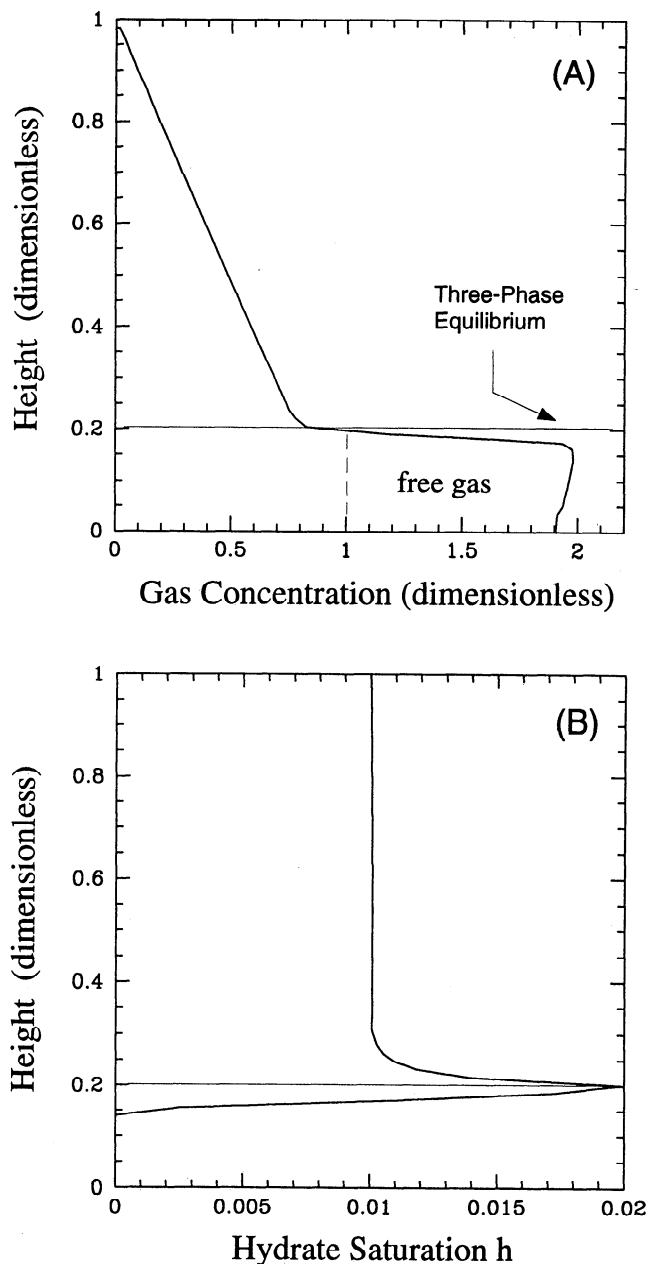

Figure 10. (a) Gas concentration and (b) hydrate saturation with depth due to sedimentation. The base of the hydrate zone has moved from $\tilde{z} = 0$ to $\tilde{z} = 0.2$ over the numerical simulation. Gas in excess of the (dimensionless) saturation $\tilde{c} = 1$ is present as free gas. The methane gas which is released by hydrate dissociation migrates back into the hydrate zone to produce a sharp peak in the saturation at the present base of the hydrate zone.

into the hydrate zone, the latent heat released by hydrate formation causes a local increase in temperature which prevents further hydrate formation until this excess heat is removed. Since the processes of sedimentation and chemical diffusion are slow compared with thermal diffusion, the latent heat is readily removed and hydrate formation occurs over a small depth range. In this case, nonequilibrium effects are primarily responsible for smearing the hydrate accumulution over a small depth.

Superimposed on the sharp increase in hydrate saturation at the base of the layer is a more gradual increase in h that occurs throughout the layer. Gas is transported upward by chemical diffusion along the concentration gradient. The result is a slow but nearly uniform increase in hydrate saturation throughout the layer. This accumulation is very similar to accumulation due to advective transport from below. The principal difference here is the presence and role of free gas below the hydrate layer. In the calculations shown in Figure 10 the excess gas released by dissociation contributes to the chemical gradient that drives diffusion into the hydrate zone. This sharp gradient at the base of the layer causes the peak in hydrate saturation. On the other hand, if any gas in excess of the solubility forms bubbles that remain trapped in the sediments, then the gas concentration in the fluid which drives chemical diffusion would be limited by the gas solubility. The smaller chemical gradient would reduce the gas transport from below and a smaller peak in the hydrate concentration would develop. In fact, the resulting profile would look quite similar to that produced by the advection model. These conclusions should be qualified since several processes have been neglected which could play an important role. One is the mobility of bubbles that nucleate from any excess gas below the hydrate zone and another is the release of buoyant freshwater by hydrate dissociation. In particular, the mobility of gas bubbles could contribute to a sharp increase in the saturation because these bubbles would not be expected to persist for very long once they enter the hydrate zone [Handa, 1990]. Both of these processes can be incorporated into the mathematical framework developed in this paper.

Conclusions

We have presented a general set of equations (1)–(5) for the formation of gas hydrates in uniform porous media. A number of solutions are obtained to elucidate the relative importance of various physical effects on hydrate formation. An analytical solution is derived for the idealized problem of hydrate growth in a porous half-space which is cooled on its boundary. Predictions for the growth rate of a hydrate layer and its volume saturation are useful for testing our theoretical development in laboratory simulations. Consideration of kinetic barriers to crystal growth suggests that nonequilib-

rium effects are negligible in natural environments but could be more important in laboratory simulations.

Numerical calculations are used to investigate two situations that are thought to be representative of formation conditions in marine sediments. One involves the biogenic production of methane within the hydrate zone. The added effect of sedimentation causes hydrate at the base of the layer to dissociate. Upward migration of the released methane produces a sharp increase in hydrate saturation at the base of the layer and a more gradual increase throughout the layer. The other problem considered in this study involves a flux of methane into the hydate zone by fluid transport from below. A simple theoretical expression is derived for the rate of hydrate accumulation which depends on the fluid velocity and the nature of the two-phase equilibrium between sea water and hydrate. For a representative phase diagram and a typical fluid velocity, we predict an additive increase in the hydrate saturation of 1% of the pore volume in 10^5 years. The vertical distribution of the hydrate saturation is largely determined by the phase diagram. Using the theoretical phase-equilibrium calculations of *Zatsepina and Buffett* (submitted manuscript, 1997), we find that hydrate forms most rapidly at the base of the layer and that the accumulation rate decreases exponentially into the hydrate zone over a distance of roughly 80–100 m. This general pattern of decreasing saturation above the base of the hydrate layer is consistent with both geophysical and geochemical estimates.

References

Abramowitz, M., and I.A. Stegun, Eds., *Handbook of Mathematical Functions*, p. 297, Dover, Mineola, N. Y., 1972.

Brooks, J.M., A.W.A. Jeffrey, T.J. McDonald, R.C. Pflaum, and K.A. Kvenvolden, Geochemistry of hydrate gas from Site 570, DSDP Leg 84, *Initial Rep. Deep Sea Drill. Proj.*, *84*, 699–703, 1985.

Cherskii, N.V., and E.A. Bondarev, Thermal method of exploiting gas-hydrated strata, *Sov. Phys. Dokl.*, *17*, 211–213, 1972.

Claypool, G.E., and I R. Kaplan, The origin and distribution of methane in marine sediments, in *Natural Gases in Marine Sediments*, edited by I.R. Kaplan, pp. 99–139, Plenum, New York, 1974.

Collett, T.S., Potential of gas hydrates outlined, *Oil Gas J.*, *90 (25)*, 84–87, 1992.

Collett, T.S., Natural gas hydrates of the Prudhoe Bay and Kuparuk River area, North Slope, Alaska, *AAPG Bull.*, *77*, 793–812, 1993.

Collins, B.P., and J.S. Watkins, Analysis of a gas hydrate off southwest Mexico using seismic processing techniques and Deep Sea Drilling Project Leg 66 results, *Geophysics*, *50*, 16–24, 1985.

Davis, E.E., R.D. Hyndman, and H. Villinger, Rates of fluid expulsion across the northern Cascadia accretionary prism: Constraints from new heat flow and multichannel seismic reflection data, *J. Geophys. Res.*, *95*, 8869-8889, 1990.

Englezos, P., N. Kalogerakis, P.D. Dholabhai, and P.R. Bishnoi, Kinetics of formation of methane and ethane gas hydrates, *Chem. Eng. Sci.*, *42*, 2647-2658, 1987.

Fogg, P.G.T., and W. Gerrard, *Solubility of Gases in Liquids*, pp. 113-159, John Wiley, New York, 1991.

Ginsburg, G.A., A.N. Kremlev, M.N. Grigor'ev, A.D. Pavlenkin, G.V. Larkin, and V.Y. Tsar'kov, The discovery of solid gas hydrate in the rock at the foot of the continental slope of the Crimea, *Trans. USSR Acad. Sci. Earth Sci. Sect.*, *309*, 83-85, 1989.

Handa, Y. P., Effect of hydrostatic pressure and salinity on the stability of gas hydrates, *J. Phys. Chem.*, *94*, 2652-2657, 1990.

Holbrook, W.S., H. Hartley, W.T. Wood, R.A. Stephen, D. Lizarralde, and Leg 164 Science Party, Methane hydrate and free gas on the Blake Ridge from vertical seismic profiling, *Science*, *273*, 1840-1843, 1996.

Hyndman, R.D., and E.E. Davis, A mechanism for the formation of methane hydrate and seafloor bottom-simulating reflectors by vertical fluid expulsion, *J. Geophys. Res.*, *97*, 7025-7041, 1992.

Hyndman, R D., and G.D. Spence, A seismic study of methane hydrate marine bottom simulating reflectors, *J. Geophys. Res.*, *97*, 6683-6698, 1992.

Hyndman, R D., K. Wang, T. Yuan, and G.D. Spence, Tectonic sediment thickening, fluid expulsion, and the thermal regime of subduction zone accretionary prisms: The Cascadia margin off Vancouver Island, *J. Geophys. Res.*, *98*, 21865-21876, 1993.

Kroos, B.M., and D. Leythaeuser, Experimental measurements of the diffusion parameters of light hydrocarbons in water-saturated sedimentary rocks II, Results and geochemical significance, *Org. Geochem*, *12*, 91-108, 1988.

Kvenvolden, K.A., Gas hydrates: Geological perspective and global change, *Rev. Geophys.*, *31*, 173-187, 1993.

Kvenvolden, K.A., and L.A. Barnard, Gas hydrates of the Blake Outer Ridge, DSDP Site 533, Leg 76, *Initial Rep. Deep Sea Drill. Proj.*, *76*, 353-366, 1983.

Lide, D.R., Ed., *CRC Handbook of Chemistry and Physics*, 71st ed., pp. 6-8, CRC Press, Boca Raton, Fl., 1990.

Loehle, C., Geologic methane as a source for post-glacial CO_2 increases: The hydrocarbon pump hypothesis, *Geophys. Res. Lett.*, *20*, 1415-1418, 1993.

Makogon, Y, F., V.I. Tsarev, and N.V. Cherskiy, Formation of large natural gas fields in zones of permanently low temperatures, *Dokl. Akad. Nauk SSSR Earth Sci.*, *205*, 215-218, 1972.

Minshull, T.A., S.C. Singh, and G.K. Westbrook, Seismic velocity structure of a gas hydrate reflector, offshore western Columbia, from full waveform inversion, *J. Geophys. Res.*, *99*, 4715-4734, 1994.

Nisbet, E.G., The end of the ice age, *Can. J. Earth Sci.*, *27*, 148-157, 1990.

Paull, C.D., W. Ussler III, and W.P. Dillon, Is the extent of glaciation limited by marine gas-hydrates?, *Geophys. Res. Lett.*, *18*, 432-434, 1991.

Paull, C.D., W. Ussler III, and W.S. Borowski, Source of methane to form marine gas hydrates, in *Natural Gas Hydrates*, edited by E.D. Sloan, J. Happel Jr., and M.A. Hnatow, Ann. N. Y. Acad. of Sci., *715*, 392-409, 1994.

Phillips, O.M., *Flow and Reactions in Permeable Rocks*, 285 p., Cambridge Univ. Press, New York, 1991.

Rempel, A., Theoretical and experimental investigations into the formation and accumulation of gas hydrate, M.Sc. thesis, Univ. of B. C., Vancouver, Canada, 1994.

Rowe, M.M., and J.F. Gettrust, Fine structure of methane hydrate-bearing sediments on the blake Outer Ridge as determined from deep-tow multichannel seismic data, *J. Geophys. Res.*, *98*, 463-473, 1993.

Selim, M.S., and E.D. Sloan, Heat and mass transfer during the dissociation of hydrates in porous media, *AIChE J.*, *35*, 1049-1052, 1989.

Singh, S.C., and T.A. Minshull, Velocity structure of a gas hydrate reflector at ocean drilling program site 889 from a global seismic waveform inversion, *J. Geophys. Res.*, *98*, 24,221-24,233, 1994.

Sincovec, R.F., and N.K. Madsen, Solution of systems of nonlinear parabolic partial differential equations in one space dimension using the method of lines, *ACM Trans. Math Software*, *1*, 261-263, 1978.

Sloan, E.D., *Clathrate Hydrates of Natural Gases*, 641 p., Marcel Dekker, New York, 1990.

Tsypkin, G.G., Dissociation of gaseous hydrates in beds, *J. Eng. Phys.*, *60*, 556-561, 1991.

Yamane, K., and I. Aya, Solubility of carbon dioxide in hydrate region at 30 MPa, Paper presented at the International Conference on Technologies for Marine Environment Preservation, The Society of Naval Architects of Japan, Tokyo, 1995.

Yuan, T., Spence, G. D., and R. D. Hyndman, Seismic velocities and inferred porosities in the accretionary wedge sediments at the Cascadia Margin, *J. Geophys. Res.*, *99*, 4413-4427, 1994.

Yuan, T., R. D. Hyndman, G. D. Spence, and B. Desmons, Seismic velocity increase and deep-sea gas hydrate concentration above a bottom-simulating reflector on the northern Cascadia continental slope, *J. Geophys. Res.*, *101*, 13,655-13671, 1996.

B.A. Buffett, Department of Earth and Ocean Sciences, 2219 Main Mall, University of British Columbia, Vancouver, B.C., Canada V6T 1Z4. (e-mail: buffett@geop.ubc.ca)

A.W. Rempel, Institute of Theoretical Geophysics, Department of Applied Mathematics and Theoretical Physics, University of Cambridge, Silver Street, Cambridge, England.